Investigating the Role of Helical Markers in 3D Catheter Shape Monitoring from 2D Fluoroscopy

A E T Yang, Jérôme Szewczyk

Investigating the Role of Helical Markers in 3D Catheter Shape Monitoring from 2D Fluoroscopy

Anne En-Tzu YANG and Jérôme SZEWCZYK

Institut des Systèmes Intelligents et de Robotique, Sorbonne Université
CC 173 - 4 Place Jussieu, 75005 Paris, FR - Tel : +33 (0)1 44 27 51 41
Contact: yang@isir.upmc.fr

This work provides preliminary results indicating that helical markers and neural networks can enable efficient monitoring of the 3D shape and orientation of an active catheter from isolated 2D fluoroscopic images.

1 Introduction

Accurate performance of minimally invasive surgeries (MIS) requires intra-operative feedback. For active catheters, particularly, it is necessary to track beyond the tip and include an extended longitudinal section so as to avoid tissue damages by unintended operations of active components along the length.

The present study aims to obtain shape and orientation of active catheters with fluoroscopy, which has been a standard protocol for catheter monitoring[1]. To overcome the limitations of 2D while avoiding the additional computational and financial costs of bi-plane imaging[2], radiopaque markers are introduced.

Publications have shown that band markers aid tip orientation tracking[3] and that helical markers aid curvature sensing[4]. This work trains a shallow neural network (NN) to reconstruct the full-length 3D configuration of an active catheter[5] from projections of designed markers. The system can potentially be generalized beyond fluoroscopy for ultrasound[6][7] or magnetic resonance imaging (MRI)[8].

2 Methods

2.1 Experimental setup and variables

A catheter prototype was made from a torque coil (Fig.1). To assist with tracking, compression springs were attached as radiopaque helices surrounding the coil. An additional copper wire looped around one end

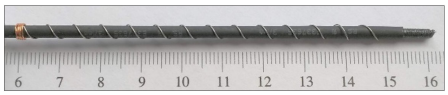

Figure 1: *A prototype of catheter and helical markers (the scale bar is in cm).*

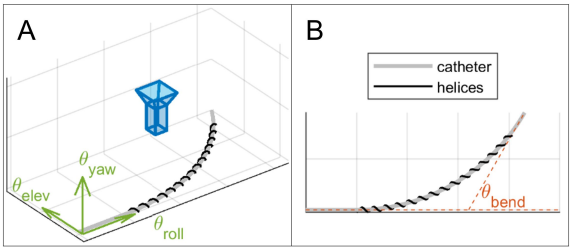

Figure 2: *(A) Three variables for orientation with respect to imaging plane (in blue) and (B) one for shape.*

of the coil to serve as a reference for base point. Images of the prototype in various shapes and orientations were acquired by Siemens' radiology system, Artis Zeego.

The orientation of a catheter can be defined by three variables– yaw, roll, and pitch (Fig. 2A). The shape of an active catheter can be approximated by a global bending angle measured between the base and the tip (Fig. 2B). This study focused on two of the variables:

Roll angle θ_{roll} is the angle about the unbent catheter's length. θ_{roll} varied between 0° and 75° in 188 increments automatically by the 20sDR-H 30 protocol on Artis Zeego.

Bending angle θ_{bend} is the difference between angles in the distal and proximal segments. In this work, the catheter was manually deflected into five different θ_{bend}.

There were, therefore, a total of 940 configurations. Note that the variations of yaw and pitch are also crucial and have been part of the work in progress (see 3.2).

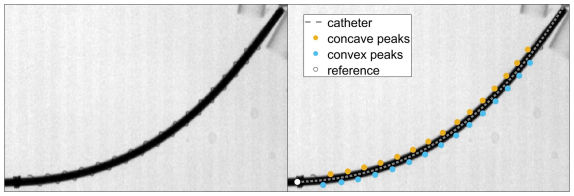

Figure 3: *An example of 2D image (left) and the image overlaid with extracted peaks, catheter shape, and reference point (right).*

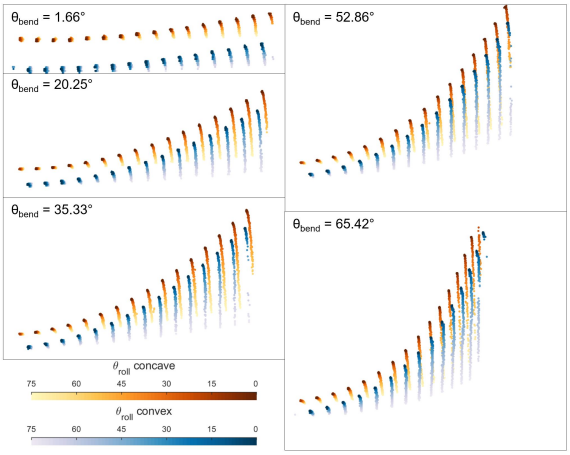

Figure 4: *The 2D trajectories of helical peaks in different roll (θ_{roll}) and bending (θ_{bend}) angles. All subplots share the same horizontal axis limit.*

2.2 Image analysis

All images were post-processed in MATLAB^{TM}. Fig. 3 shows an example frame before and after processing. The projected shape of the catheter was approximated as a 3^{rd}-order polynomial. Helical peaks were identified by two methods. The first method found regions of connected pixels and retained those in proper sizes. In each region, the pixel furthest away from the catheter was labeled as a peak. Nevertheless, due to θ_{bend} and projection perspective, not all peaks displayed as closed areas to be identifiable with the first method. The second method, based on the Qhull algorithm[9], searched for points which formed the greatest convex hull around the catheter. After eliminating overlaps and falsely identified peaks by thresholding inter-peak and peak-to-catheter distances, the trajectories of peaks over θ_{roll} are shown in each subplot in Fig. 4 for each θ_{bend}.

3 Results

3.1 Neural network prediction

Each catheter configuration yielded about two dozens of x- and y- of helical peaks. The information of each set of peaks was consolidated into single variables. To uniquely recognize the two catheter configuration variables (θ_{bend} and θ_{roll}), it is expected that a minimum of two predictors are needed.

A two-layer feedforward network was trained with a

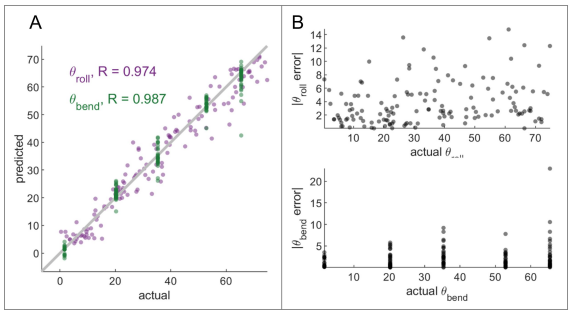

Figure 5: *(A) The correlation of θ_{roll} and θ_{bend} between neural network output (predicted) and ground truth (actual). (B) The absolute errors of θ_{roll} (top) and θ_{bend} (bottom) predictions.*

nonlinear least square fitting algorithm[10]. All data were divided randomly into training (70%), validating (15%), and testing (15%) sets. Different predictors were tested in a number of sessions. The two predictors resulting in the best shape recognition were– d_0 (longitudinal distance between the most proximal marker and the reference point) and $\overline{d_{i1}} - \overline{d_{i2}}$ (difference between concave and convex average inter-peak distances).

The correlations between predicted and actual θ_{bend} and θ_{roll} of the testing set ($n = 141$) are depicted in Fig. 5A. The errors of both variables are plotted in Fig. 5B. Almost all errors are under 15°, and neither of the errors seem to display any trends of variation.

3.2 Discussions

A significant contribution of the present work is the recognition of large θ_{bend} at large θ_{roll} (e.g. bright markers in the fifth subplot in Fig. 4), an ambiguity primarily introduced by θ_{roll}. The markers does not interfere with the incision in cases where the markers are covered with an external layer[5]. It is also worth noting that the present study attempted a framework without regard to the perturbation of the table and the calibration of the projection perspective.

Several aspects still need to be addressed. Improved image quality and processing may resolve the small portion of missing or erroneous peaks in the current results. Moreover, simulation covering a broader variety of possible configurations is expected to robustize neural network performance. Presently, θ_{bend} variation was limited to five distinct values.

As mentioned in 2.1, future work is ongoing to expand the model to include θ_{yaw} and θ_{pitch} variations. Separate simulations supported the validity of θ_{pitch} recognition with the addition of one predictor– coefficient of variation of inter-peak distances. As for θ_{yaw}, parallel to the imaging plane, it is expected to be correlated with the overall x-y slopes.

In summary, to achieve efficient shape and orientation identification of a 3D catheter with single-plane fluoroscopy, the present work demonstrated the potential of neural network and helical markers.

*The authors thank Dr. Pascal Haigron and Mr.

Miguel Castro for their assistance with image acquisition at Centre Hospitalier Universitaire de Rennes. This work was supported by French state funds managed by the ANR within the Investissements d'Avenir programme (Labex CAMI) under reference ANR-11-LABX-0004.

References

[1] C. E. Metz and L. E. Fencil, "Determination of three-dimensional structure in biplane radiography without prior knowledge of the relationship between the two views: Theory," Med. Phys., vol. 16, no. 1, pp. 45–51, 1989.

[2] S. A. M. Baert, E. B. van de Kraats, T. van Walsum, M. A. Viergever, and W. J. Niessen, "Three-dimensional guide-wire reconstruction from biplane image sequences for integrated display in 3-D vasculature," IEEE Transactions on Medical Imaging, vol. 22, no. 10, pp. 1252–1258, Oct. 2003.

[3] S. Hwang and D. Lee, "3D Pose Estimation of Catheter Band Markers based on Single-Plane Fluoroscopy," in 2018 15th International Conference on Ubiquitous Robots (UR), 2018, pp. 723–728.

[4] R. Xu, A. Yurkewich, and R. V. Patel, "Curvature, Torsion, and Force Sensing in Continuum Robots Using Helically Wrapped FBG Sensors," IEEE Robotics and Automation Letters, vol. 1, no. 2, pp. 1052–1059, Jul. 2016.

[5] T. Couture and J. Szewczyk, "Design and Experimental Validation of an Active Catheter for Endovascular Navigation," *Journal of Medical Devices*, vol. 12, no. 1, pp. 011003-011003–12, Nov. 2017.

[6] J. Stoll, H. Ren, and P. E. Dupont, "Passive Markers for Tracking Surgical Instruments in Real-Time 3-D Ultrasound Imaging," IEEE Transactions on Medical Imaging, vol. 31, no. 3, pp. 563–575, Mar. 2012.

[7] J. Guo, C. Shi, and H. Ren, "Ultrasound-Assisted Guidance With Force Cues for Intravascular Interventions," IEEE Transactions on Automation Science and Engineering, vol. 16, no. 1, pp. 253–260, Jan. 2019.

[8] S. Zuehlsdorff et al., "MR coil design for simultaneous tip tracking and curvature delineation of a catheter," Magn. Reson. Med., vol. 52, no. 1, pp. 214–218, Jul. 2004.

[9] C. B. Barber, D. P. Dobkin, D. P. Dobkin, and H. Huhdanpaa, "The Quickhull Algorithm for Convex Hulls," ACM Trans. Math. Softw., vol. 22, no. 4, pp. 469–483, Dec. 1996.

[10] M. T. Hagan and M. B. Menhaj, "Training feedforward networks with the Marquardt algorithm," IEEE Transactions on Neural Networks, vol. 5, no. 6, pp. 989–993, Nov. 1994.